Title

Case Studies in Nanocluster Synthesis and Characterization: Challenges and Opportunities

Journal

Accounts of Chemical Research, 51(10)

ISSN

0001-4842

Authors

Cook, Andrew W

Hayton, Trevor W

Publication Date

2018-10-16

DOI

10.1021/acs.accounts.8b00329

Peer reviewed

Case Studies in Nanocluster Synthesis and Characterization: Challenges and Opportunities

Andrew W. Cook and Trevor W. Hayton*

Department of Chemistry and Biochemistry, University of California, Santa Barbara, California 93106, United States

Atomically Precise Nanoclusters (APNCs) are an emerging area of nanoscience. Their mono-dispersity and well-defined arrangement of capping ligands facilitates the interrogation of their fundamental physical properties, allowing for the development of structure-function relationships, as well as their optimization for a variety of applications, including quantum computing, solid-state memory, catalysis, sensing, and imaging. However, APNCs present several unique synthetic and characterization challenges. For example, nanocluster syntheses are infamously low yielding and often generate complicated mixtures. This combination of factors makes nanocluster purification and characterization more difficult than that of typical inorganic or organometallic complexes. Yet, while this fact is undoubtedly true, the past lessons learned from the characterization of inorganic complexes are still useful today.

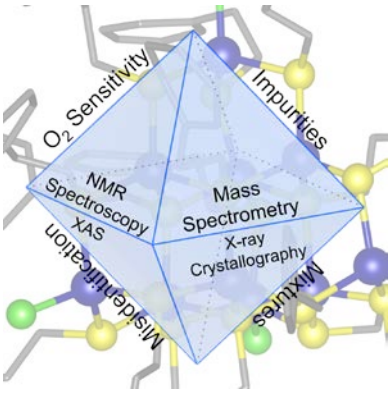

In this Account, we discuss six case studies taken from the recent literature in an attempt to identify common challenges and pitfalls encountered in APNC synthesis and characterization. For example, we show that several reducing agents employed in APNC synthesis, including the commonly used reagent $NaBH_4$, do not always behave as anticipated. Indeed, we highlight one case where $NaBH_4$ reduces the ligand and not the metal center, and other cases where $NaBH_4$ acts as a Brønstead base instead of a reducing agent. In addition, we have identified several instances where the use of phase transfer agents, which were added to mediate APNC formation, played no role in the nanocluster synthesis, and likely made the isolation of pure material more difficult. We have also identified several cases of cluster misidentification driven by spurious or ambiguous characterization data, most commonly collected by mass spectrometry. To address these challenges, we propose that the nanocluster community adopt a standard protocol of characterization, similar to those used by the organometallic and coordination chemistry communities. This protocol requires that many complementary techniques be used in concert to confirm formulation, structure, and analytical purity of APNC samples. Two techniques that are under-utilized in this regard are combustion analysis and NMR spectroscopy. NMR spectroscopy, in particular, can provide information on purity and formulation that are difficult to collect with any other technique. X-ray absorption spectroscopy is another powerful method of nanocluster characterization, especially in cases where single crystals for X-ray diffraction are not forthcoming. Chromatographic techniques can also be extremely valuable for assessing purity, but are rarely used during APNC characterization. Our goal with this Account is to begin a discussion with respect to the best protocols for nanocluster synthesis and characterization. We believe that embracing a standard characterization protocol would make APNC synthesis more reliable, thereby accelerating their integration into a variety of technologies.

INTRODUCTION

The synthesis and study of Atomically Precise Nanoclusters (APNCs) is an emerging area of nanoscience.[1-3] Unlike traditional nanoparticles, APNCs are mono-disperse and feature a well-defined arrangement of capping ligands. This high level of chemical precision allows for the development of structure-function relationships, permitting their rapid optimization for a variety of applications, including quantum computing,[4] solid-state memory,[5] catalysis,[6-8] sensing,[9] and imaging.[9,10] The high degree of chemical precision also allows for the interrogation of fundamental physical properties, such as the number of gold atoms required for the onset of metallic character.[11]

Many materials fall under the APNC umbrella, which are defined here as a group of metal or metalloid atoms that approaches or exceeds 1 nm in diameter in at least one dimension.[12] For example, APNCs are known for group II-IV semiconducting materials,[13,14] group III-V semi-conducting materials,[15] metal chalcogenides,[16,17] and metal oxides.[18] However, recent nanocluster work has largely focused on low oxidation state clusters, which feature considerable amounts of metal-metal bonding.[1,2] It is these types of clusters, i.e., nanoclusters with some formal M(0) character, that will be the primary focus of this Account.

Nanocluster synthesis and characterization is a rapidly growing field. Approximately 1000 nanoclusters papers were published in 2016, which is a nearly 100 fold annual increase since 1996.[2] As with any rapidly developing field, however, there have been some growing pains. This is partly a consequence of the materials themselves, as APNCs present several unique synthesis and characterization challenges. For example, in some instances single crystal X-ray data are not of sufficiently high quality to accurately determine the number and arrangement of the surface-capping ligands.[13] Additionally, transmission electron microscopy, which works well for the characterization of larger nanoparticles, is known to cause structural changes to some nanoclusters.[19] Moreover, and of particular relevance to this Account, nanocluster syntheses are infamously low yielding and often generate complicated mixtures. This combination of factors makes nanocluster purification and characterization difficult.[20] Indeed, impurities in nanocluster samples significantly complicate the construction

of structure-function relationships, as recently demonstrated by Choi *et al.* in their attempts to correlate structure and nuclearity with photoluminescence behavior.[21] This is also perhaps why several archetypal gold nanoclusters were initially mischaracterized, including $[Au_{25}(SCH_2CH_2Ph)_{18}]^-$, $[Au_{38}(SCH_2CH_2Ph)_{24}]$, and $[Au_{144}(SCH_2CH_2Ph)_{60}]$.[1]

The APNC field is not the first to deal with these challenges, which are actually as old as synthetic chemistry itself. In this regard, it is insightful to survey the best practices previously developed for the characterization of organometallic and inorganic compounds. A good summary of these practices, as well as some interesting case studies, can be found in "The Synthesis and Characterization of Inorganic Compounds".[22] These best practices have also been codified in the "Information for Authors" of several journals.[23,24] While these practices were originally developed for inorganic synthesis, the past lessons learned are still useful today. In this Account, we highlight how these past lessons can help avoid several common pitfalls and challenges encountered in nanocluster synthesis and characterization. The format of this account follows the case studies approach used effectively in Finke's 1999 nanocluster review.[19] We believe that this analysis is both timely and appropriate because APNC synthesis is still a young field and no standard characterization protocol has yet been agreed upon.

Case Study #1: Synthesis of $Cu_8(MPP)_4$

In 2011, Chen and co-workers reported the synthesis of the Cu nanocluster, $Cu_8(MPP)_4$ (HMPP = 2-mercapto-5-*n*-propylpyrimidine).[25] This cluster was synthesized using a one-phase Brust-Schiffrin protocol. Specifically, a mixture of $Cu(NO_3)_2$ and $[N(Oct)_4][Br]$, in EtOH, was treated with HMPP and excess $NaBH_4$ (Scheme 1a). The resulting Cu_8 nanocluster was isolated by precipitation and centrifugation, but no yield was reported. Evidence for the $Cu_8(MPP)_4$ formulation came primarily from ESI-MS, specifically the identification of a parent ion peak, $[Cu_8(MPP)_4 + H]^+$, at 1120 *m/z*. However, there are several problems with this assignment. First, $[Cu_8(MPP)_4 + H]^+$ should feature a parent peak at 1121 *m/z*, not 1120 *m/z*. Additionally, a detailed isotopic distribution analysis was not provided for this feature, complicating attempts to evaluate the mass spectral assignment.

Scheme 1. Reported syntheses of MPP-protected Cu nanoclusters, as described in References 25 and 30.

Chen and co-workers, 2011:

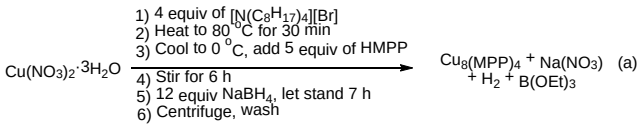

Hayton and co-workers, 2017:

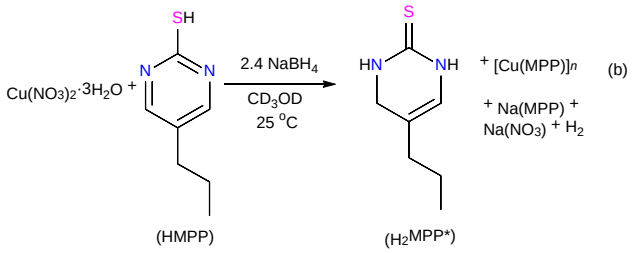

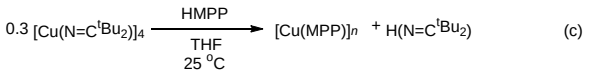

Given our interest in copper nanoclusters,[8,26-29] we endeavored to re-synthesize $Cu_8(MPP)_4$,[30] taking great care to match the reported reaction conditions as closely as possible. In our hands, however, the reaction of $Cu(NO_3)_2$ with $[N(C_8H_{17})_4][Br]$, HMPP, and excess $NaBH_4$, in EtOH, resulted in formation 2-mercapto-5-*n*-propyl-1,6-dihydropyrimidine (H_2MPP^*) as the major product. This material was formed by reduction of the pyrimidine ring in HMPP by $NaBH_4$. Moreover, we observed no evidence for the formation of a Cu_8 nanocluster in the reaction mixture.

We also monitored the reaction of $Cu(NO_3)_2$ with HMPP and $NaBH_4$, in CD_3OD, by ^1H NMR spectroscopy (Scheme 1b). Under these conditions, we still observed formation of H_2MPP^* as the major product, as expected. We also observed formation of Na(MPP) and $[Cu(MPP)]_n$ as minor components of the reaction mixture. The formation of $[Cu(MPP)]_n$ was confirmed by its independent synthesis via reaction of $[Cu(N=C^tBu_2)]_4$ with 3.6 equiv of HMPP, in THF (Scheme 1c). It was characterized by a wide variety of methods, including ^1H NMR spectroscopy, X-ray crystallography (Figure 1), and ESI-MS. $[Cu(MPP)]_n$ appears to exist as a mixture of oligomers in solution, but crystallizes from solution as a hexamer, $[Cu(MPP)]_6$. It is possible that this cluster, along with H_2MPP^*, were present in the material isolated in 2011, but neither was mentioned in the original report.

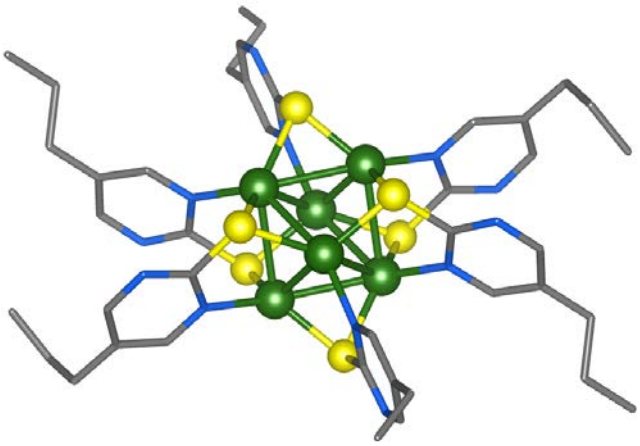

Figure 1. Ball-and-stick diagram showing the solid-state structure of $[Cu(MPP)]_6$. Color legend: copper, green; sulfur, yellow; carbon, grey; nitrogen, blue.

Several important lessons can be gleaned from this case study. Most importantly, it appears that the identification of $Cu_8(MPP)_4$ as a reaction product was driven largely by an over-reliance on mass spectrometry data. While ESI-MS is an important characterization tool for APNCs,[1] it does have several limitations that must be considered when using this technique. Most importantly, the intensity of a peak in the mass spectrum does not necessarily correlate with that ion's concentration in the bulk sample. Indeed, many factors play a role in determining peak intensity, including the analyte's sensitivity coefficient *k*, the dielectric constant of the solvent, the presence of electrolytes, and the instrument settings.[31] Consequently, it is clear that ESI-MS cannot be used to assess bulk purity. It is also clear that some species could be silent by ESI-MS. The latter point is well illustrated by another example from this system. Specifically, we could not observe H_2MPP^* in the reaction mixture by ESI-MS, despite our best efforts, and despite the fact that it was the major product from the reaction of $Cu(NO_3)_2$ with HMPP and $NaBH_4$.[30]

Another take-away is the important role that ^1H NMR spectroscopy played in the identification of the reaction products, in particular H_2MPP^*. Multinuclear NMR spectroscopy remains an underutilized technique in diamagnetic and paramagnetic nanocluster characterization, despite its many advantages. NMR spectroscopy is unique amongst characterization techniques in its ability to provide information on the number and relative ratios of capping ligand environments. NMR spectroscopy is also non-destructive and can quickly reveal the presence of organic impurities, such as free supporting ligand, in nanocluster samples.

Case Study #2: Thiolate-protected Ni Nanoclusters

In 2014, Xu and co-workers reported the synthesis of two large Ni nanoclusters, $[Ni_{39}(SCH_2CH_2Ph)_{24}]$ and $Ni_{41}(SCH_2CH_2Ph)_{25}]$.[32] These were synthesized by reaction of $NiCl_2{\cdot}6H_2O$, dissolved in THF and MeOH, with a mixture of $PhCH_2CH_2SH$ and aqueous $NaBH_4$ (Scheme 2a). The resulting Ni clusters were characterized by MALDI-TOF, XPS, UV-vis spectroscopy, and magnetometry. However, neither a crystal structure nor a yield was reported.

Curiously, at about the same time, several other research groups investigated the reaction of $NiCl_2$ with $PhCH_2CH_2SH$ and $NaBH_4$, under Brust-Schiffrin conditions.[33-35] Each group reported the formation of a Ni(II) thiolate coordination polymer $[Ni(SCH_2CH_2Ph)_2]_6$ as the major product (Scheme 2), while one group also isolated a smaller cluster, $[Ni(SCH_2CH_2Ph)_2]_4$, using slightly different conditions.[34] These products are clearly very different from the mixed-valent Ni_{39} and Ni_{41} nanoclusters reported in 2014, despite the similar reaction protocols.

Scheme 2. Reported syntheses of thiolate-protected Ni nanoclusters, as described in References 32, 33, and 35.

Xu and co-workers, 2014:

$NiCl_2{\cdot}(H_2O)_6$ → 1) Dissolve in MeOH (2mL) and THF (10 mL); 2) Add 5 equiv of $PhCH_2CH_2SH$; 3) Add 10 equiv of $NaBH_4$(aq); 4) Stir 60 h, filter, rinse with MeOH/H_2O → $Ni_{39}(SR)_{24}$ + $Ni_{41}(SR)_{25}$, R = CH_2CH_2Ph, **no yield reported** (a)

Bernhard and co-workers, 2013:

$NiCl_2{\cdot}(H_2O)_6$ → 1) Add 2 equiv of $[N(Oct)_4][Br]$; 2) Dissolve in THF (100 mL); 3) Add 5 equiv of $PhCH_2CH_2SH$; 4) Add 10 equiv of $NaBH_4$(aq); 5) Stir 24 h, concentrate, rinse with MeOH; 6) Extract with CH_2Cl_2; 7) Recrystallize from CH_2Cl_2/EtOH → $[Ni(SR)_2]_6$, R = CH_2CH_2Ph, **30-35% yield** (b)

Wu and co-workers, 2014:

$Ni(NO_3)_2{\cdot}(H_2O)_6$ → 1) Add 2 equiv of $[N(Oct)_4][Br]$; 2) Dissolve in THF (25 mL); 3) Add 6 equiv of $PhCH_2CH_2SH$; 4) Add 10 equiv of $NaBH_4$(aq); 5) Stir 20 h, concentrate, wash with MeOH/H_2O; 6) Recrystallize from CH_2Cl_2/EtOH → $[Ni(SR)_2]_6$, R = CH_2CH_2Ph, **30% yield** (c)

Both $[Ni(SCH_2CH_2Ph)_2]_6$ and $[Ni(SCH_2CH_2Ph)_2]_4$ were characterized by X-ray crystallography. $[Ni(SCH_2CH_2Ph)_2]_6$ features an attractive "tiara-like" structure, wherein each thiolate ligand bridges between two Ni centers, and each Ni centers displays a square planar coordination geometry (Figure 2). Many similar Ni(II) thiolate clusters have been reported previously.[36-38]

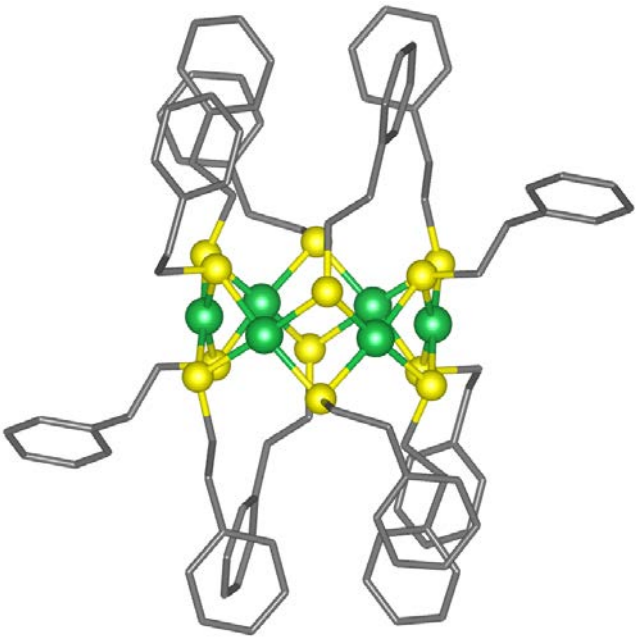

Figure 2. Ball-and-stick diagram showing the solid-state structure of $[Ni(SCH_2CH_2Ph)_2]_6$. Color legend: nickel, green; sulfur, yellow; carbon, grey.

Given the similarity of the reaction conditions employed by the four different research groups, it is worth examining why such disparate outcomes were reported. The strongest evidence to support the Ni_{39} and Ni_{41} formulations comes from MALDI-TOF data. In particular, parent peaks were observed for both ions.[32] However, given that the MALDI-TOF signal does not correlate with bulk concentration, it is possible that these species are only minor products of the reaction. In this regard, we postulate that the Ni_6 cluster was actually the major product of this transformation. Indeed, the UV-vis spectra reported for the Ni_{39}/N_{41} mixture is essentially identical to that reported for Ni_6.[34,35]

The use of the Brust-Schiffrin protocol in the synthesis of Ni_6 is also worthy of comment (Scheme 2). The Brust-Schiffrin protocol is often used in the synthesis of gold nanoclusters,[39] where phase transfer reagents, such as $[N(Oct)_4][Br]$, are thought to solubilize the Au(I) intermediates that are precursors to the reduced Au nanocluster.[40] However, not all nanocluster syntheses will benefit from Brust-Schiffrin conditions. In the case of Ni_6, for example, phase transfer reagents are likely unnecessary. To support this assertion, we note that many similar Ni(II) thiolate clusters, including $[Ni(SPh)_2]_x$ (x = 9, 11), $[Ni(SCH_2C(O)OEt)_2]_8$, and $[Ni(SCH_2CH_2{}^iPr)_2]_6$, have been previously reported, and these were synthesized using standard organometallic metathetical protocols.[36-38] Thus, while one- and two-phase Brust-Schiffrin protocols can be beneficial for nanoparticle syntheses, there is no reason to believe that Brust-Schiffrin is necessary for the synthesis of the Ni_6 cluster. In the end, the utilization of Brust-Schiffrin protocol in this example likely only makes it more difficult to generate pure material.

Case Study #3: Histidine-Stabilized Gold Nanoclusters

In 2011, Chen and co-workers reported the synthesis of a histidine-stabilized Au_{10} cluster, $[Au_{10}(His)_{10}]$.[41] The reported synthetic procedure is remarkably simple, involving the reaction of $HAuCl_4$ with 30 equiv of histidine, in H_2O, followed by incubation at room temperature for 1 h (Scheme 3a). The Au_{10} formulation was supported by ESI-MS and XPS, and based on these data, the authors concluded that the reaction produced "mono-disperse" Au_{10} nanoclusters. The apparent ease of preparation makes Au_{10} an attractive nanocluster for further applications development; however, no yield was reported.

Scheme 3. Reported syntheses of Histidine-stabilized Au nanoclusters, as described in References 41 and 20.

Chen and co-workers, 2011:

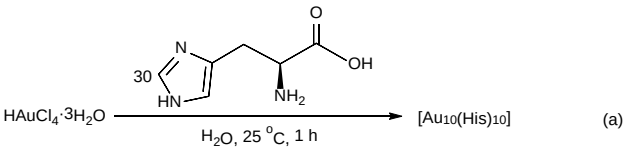

Choi and co-workers, 2013:

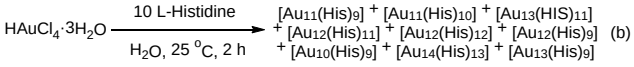

This system was re-analyzed by Choi and co-workers in 2013, and found to be substantially more complicated than originally suggested (Scheme 3b).[20] In particular, the reaction products were analyzed with reverse phase high-performance liquid chromatography (RP-HPLC) coupled with MALDI-TOF MS and ESI-MS. The RP-HPLC trace revealed at least nine histidine-stabilized Au nanoclusters were present in solution (Figure 3), ranging in size from $[Au_{10}(His)_9]$ to $[Au_{14}(His)_{13}]$, with $[Au_{12}(His)_9]$ being the major product. Unsurprisingly, unreacted histidine was also present in the sample. Interestingly, these products are similar in composition to $[Au_{10}(His)_{10}]$ (Scheme 3a), the formulation suggested in 2011.[41] However, the original characterization by ESI-MS, UV-vis spectroscopy, and XPS would have been unable to identify the presence of a complicated mixture.

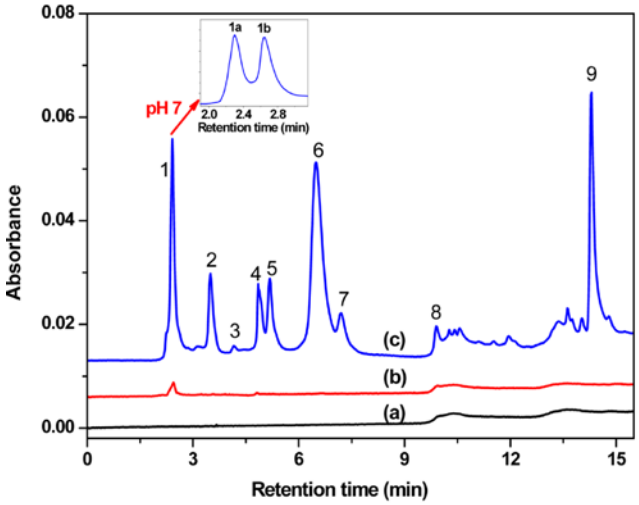

Figure 3. RP-HPLC trace of a His-stabilized Au nanocluster sample under gradient elution (blue trace). Curves a (black trace) and b (red trace) are the solvent and histidine controls, respectively. Reproduced with permission from ref. 20. © 2013 American Chemical Society.

The Choi group has used RP-HPLC to probe the outcomes of several other nanocluster reactions.[21,42] For example, they determined that reduction of $HAuCl_4$ with DMF results in formation of a complex mixture of Au nanoclusters, confirming the original finding of Kawasaki and co-workers.[43] At least 12 Au-containing nanoclusters are formed in this reaction, with $[Au_{10}(DMF)_9]^+$ and $[Au_{10}(DMF)_7]$ being the most abundant.[21] Although, it is worth noting that "surfactant-free" or "solvent-only" nanoclusters is a somewhat controversial topic.[44,45] More significantly, these results demonstrate the promise of RP-HPLC for APNC characterization, and suggest that this technique should be adopted more broadly.

Case Study #4: Monolayer-Protected $Co_x(SCH_2CH_2Ph)_m$ Nanoclusters

In 2017, Barrabés and co-workers reported the synthesis of the monolayer-protected cobalt nanoclusters, $Co_x(SCH_2CH_2Ph)_m$.[46] These were made by reaction of $CoCl_2$ and $PhCH_2CH_2SH$ (3 equiv), dissolved in THF, with an aqueous solution of $NaBH_4$ (9 equiv) (Scheme 4a). The cobalt nanoclusters were purified via filtration and extraction into CH_2Cl_2. No yield was reported. On the basis of MALDI-MS data, it was posited that the clusters ranged in size from 25 to 30 Co atoms, and they offered $Co_{25}(SR)_{18}$ and $Co_{30}(SR)_{16}$ as possible formulations. However, specific formulae to the observed peaks in the MALDI mass spectrum were not assigned.

Scheme 4. Reported synthesis of monolayer-protected cobalt nanoclusters, as described in References 46 and 47.

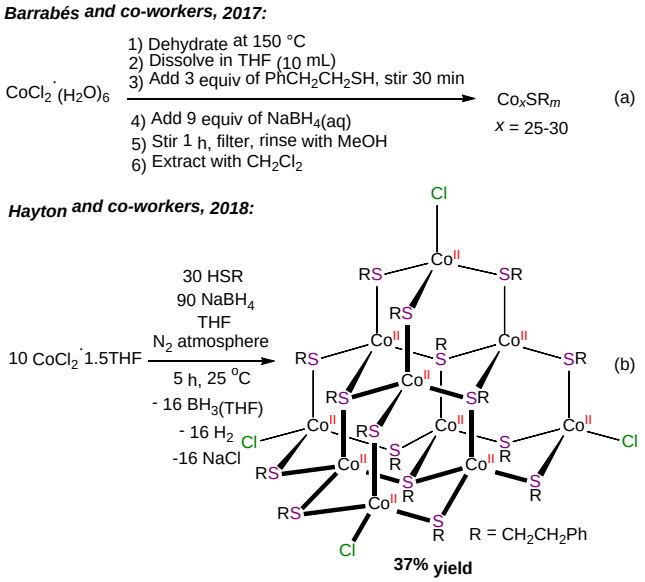

Given the rarity of well-defined metallic cobalt APNCs, we endeavored to replicate the reported synthetic procedure and continue the characterization of the product(s).[47] In our hands, the reaction of $CoCl_2$ and $HSCH_2CH_2Ph$ with $NaBH_4$, in THF under an inert atmosphere, resulted in the formation of a single cobalt-containing species (Scheme 4b), which was determined to be the T3 supertetrahedral cluster $[Co_{10}(SCH_2CH_2Ph)_{16}Cl_4]$ by X-ray crystallography (Figure 4). Importantly, we do not observe the formation of any low-valent Co-containing species in the reaction mixture. Thus, it appears that $NaBH_4$ is solely acting as a Brønstead base in this transformation, and not as a reducing agent, as originally surmised.

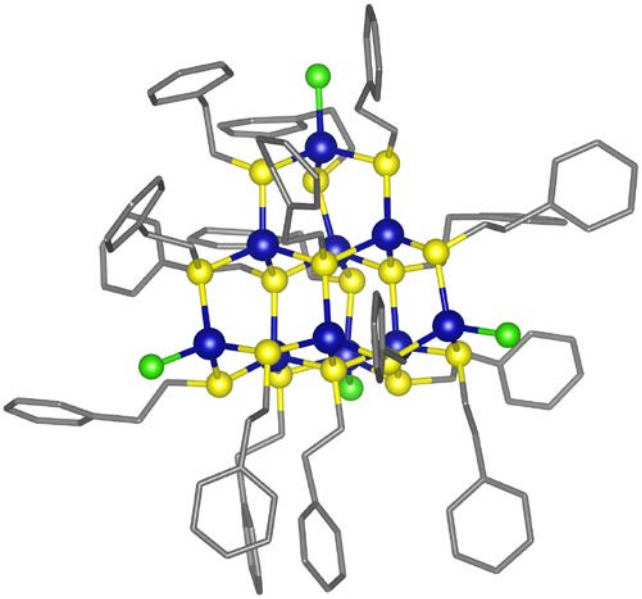

Figure 4. Ball-and-stick diagram showing the solid-state structure of $[Co_{10}(SCH_2CH_2Ph)_{16}Cl_4]$. Color legend: cobalt, blue; sulfur, yellow; carbon, grey; chlorine, green.

Interestingly, during the course of our studies, we discovered that Co_{10} is quite air sensitive. Thus, to account for the widely different reaction outcomes (Scheme 4), we hypothesize that Co_{10} was also formed in the original reaction; however, upon work-up in air, the sample reacted with O_2 to generate a mixed-ligand $Co_xO_y(SR)_m$-type cluster (or clusters). Several other groups have also noted that cobalt-thiolate complexes are generated during attempts to make Co(0) APNCs.[48,49] For example, a 2008 report claimed that reaction of Co^{2+} with $NaBH_4$, in the presence of thiol, led to the formation of cobalt nanoparticles.[50] However, Kitaev later demonstrated that the actual products from this reaction were just simple Co(II) thiolates.[49]

Interestingly, the presence of O_2 during nanocluster formation is not always harmful. In some instances, such as for the synthesis of $[Au_{25}(SCH_2CH_2Ph)_{18}]^-$, it is actually required. In this case, oxygen initiates cluster etching by formation of thiyl radicals.[51-53] In the case of Co, however, it is clear that O_2 is detrimental to the formation of a tractable product. The disparate roles of oxygen in these two systems can be readily explained by the different reduction potentials of Co^{2+} and Au^+,[54] as well as their different M-S bond strengths (Co-S = 340 kJ/mol vs. Au-S = 420 kJ/mol).[55] Overall, this case study highlights the need for rigorously air free conditions during the synthesis and work-up of APNCs of the more electropositive transition metals (e.g., Fe, Co, and Ni.)

Case Study #5: Surfactant-Free Platinum Nanoclusters

In 2010, Kawasaki and co-workers reported a simple procedure for the synthesis of "surfactant-free" Pt nanoclusters.[56] These clusters were made by thermolysis of an aqueous solution of H_2PtCl_6 in DMF, which acts as both reductant and stabilizing ligand (Scheme 5). No yield was reported, nor were the reaction by-products identified. The clusters were found to range in size from Pt_4 to Pt_6 on the basis of MALDI-MS; however, it was clear from the MS data that the clusters had reacted with the 2-mercapto-benzothiazole matrix. Thus, it is not readily apparent if the MALDI-MS data accurately represented the solution phase speciation. The oxidation state of the clusters was probed with XPS. Specifically, the authors observed a Pt $4f_{7/2}$ peak at 72.8 eV, which they interpreted as evidence for Pt(0) (The $4f_{7/2}$ peak for Pt metal appears at 71.1 eV). However, this energy is also similar to those reported for molecular Pt(II) complexes.[57]

Scheme 5. Synthesis of DMF-stabilized Pt nanoclusters, as described in Reference 56.

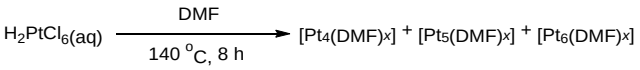

Duchesne and Zhang repeated the synthesis of these Pt nanoclusters, and then probed their local structure by X-ray absorption spectroscopy (XAS).[57] An analysis of the EXAFS spectra revealed a decrease in the Pt coordination number from 6 to 4 over the course of the reaction, consistent with reduction of the Pt(IV) ions to Pt(II) (Figure 5). Moreover, the EXAFS data showed no apparent Pt–Pt scattering path, while the XANES data indicated the average oxidation state of platinum was +2. Given these data, Zhang and Duchesne concluded that this reaction resulted in formation of small Pt(II)-containing clusters, and not the formation of Pt(0) nanoclusters, as originally suggested.

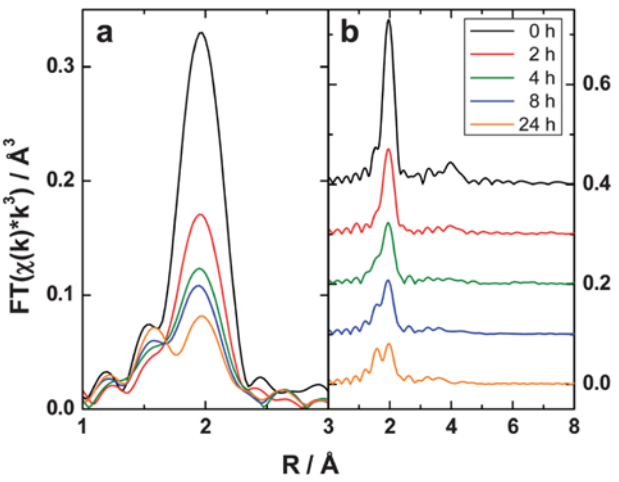

Figure 5. Pt L_3-edge EXAFS spectra of DMF-stabilized Pt nanoclusters as a function of time. Reproduced with permission from ref. 57. © 2012 Royal Society of Chemistry.

This example highlights the power of XAS in nanocluster characterization. XAS can provide insight into the size and shape of metal nanoclusters, the average oxidation state of the metal core, and the identity of the ligand shell, even when single crystals are not available. Several other groups have also used XAS to characterize nanoclusters. For example, our laboratory used EXAFS to confirm that the mixed-valent copper nanocluster $[Cu_{20}(CCPh)_{12}(OAc)_6]$ maintained its nuclearity upon deposition on to silica.[8] Similarly, Petty and coworkers used XANES to confirm the 6+ overall charge of a DNA encapsulated Ag_{10} cluster, which was consistent with their mass spectrometry measurements.[58] However, it must be noted that XAS, like any other characterization method, must be used in tandem with other techniques. In addition, because it is a bulk technique, XAS is sensitive to the presence of impurities. Therefore great care must be made to confirm sample purity before any measurements are taken.

Case Study #6: Synthesis of a Hydride-Stabilized Cu_{14} Nanocluster

In 2015, we reported the synthesis of $[Cu_{14}H_{12}(phen)_6(PPh_3)_4][Cl]_2$, formed by reaction of $[(Ph_3P)CuH]_6$ and 1,10-phenanthroline in CH_2Cl_2 (Scheme 6).[26] This cluster was isolated in 80% yield. Cu_{14} is notable for being a rare example of a copper hydride nanocluster stabilized solely by neutral donor ligands (e.g., phen and Ph_3P). Its formation from $[(Ph_3P)CuH]_6$ involves several steps, including Ph_3P ligand exchange and hydride metathesis with the CH_2Cl_2 solvent, which was ultimately determined to be the source of the two chloride counterions.

Scheme 6. Synthesis of a Cu_{14} nanocluster, as described in Reference 26.

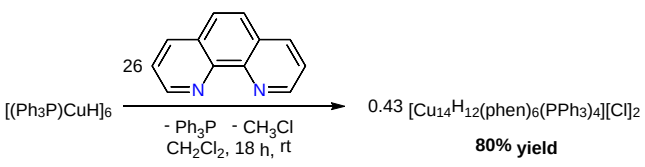

In the solid state, Cu_{14} is structured around $[Cu_4]^{4+}$ core and features T_d symmetry (Figure 6). As a result, all 12 hydride ligands are equivalent by symmetry. While the hydride ligands were not found by X-ray crystallography, DFT calculations suggest that the 12 hydride ligands occupy the outer surface of the Cu_{14} cluster. Each hydride ligand features a μ_3 coordination mode, according to the calculations, which is a common binding mode for copper hydrides.[59]

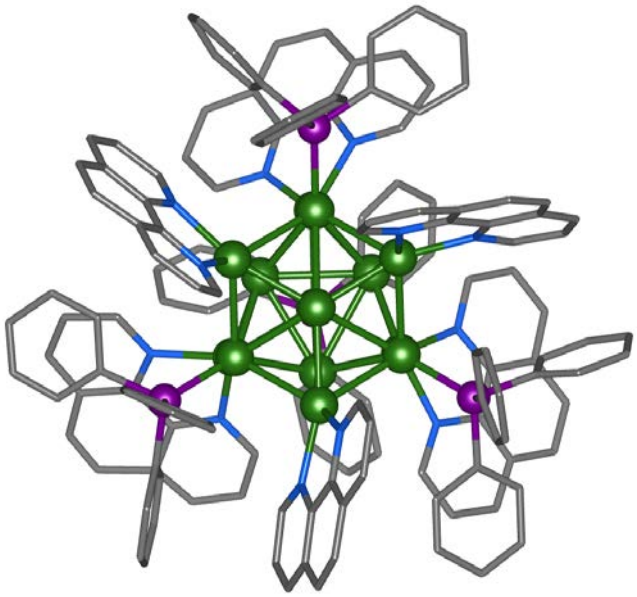

Figure 6. Ball-and-stick diagram showing the solid-state structure of $[Cu_{14}H_{12}(phen)_6(PPh_3)_4][Cl]_2$. Color legend: copper, green; phosphorus, purple; nitrogen, blue; carbon, grey. The two Cl^- counterions were removed for clarity.

Despite an analysis of its structure by X-ray crystallography, Cu_{14} proved to be quite challenging to completely characterize. In particular, the metrical parameters of its tetrahedral $[Cu_4]^{4+}$ core were found to be nearly identical to those of the tetrahedral $[Cu_4(\mu_4\text{-}H)]^{3+}$ core in $[Cu_8H\{S_2CN^nPr_2\}_6]^+$.[60] Given this similarity, we were concerned that Cu_{14} also possessed a μ_4-H ligand, which we could not detect by ^{1}H NMR spectroscopy or X-ray crystallography. Inclusion of a μ_4-H ligand into the Cu_{14} structure would alter its formula only slightly; increasing the number of hydride ligands by one and decreasing the number of chloride ligands accordingly to maintain charge balance. Because the chloride ligands in Cu_{14} were disordered over eight sites, and because hydride ligands are generally transparent to X-rays, our X-ray crystallographic data could not definitively rule out the alternative formulation, e.g., $[Cu_{14}H_{13}(phen)_6(PPh_3)_4][Cl]$.

Thus, to further support our proposed formula, we synthesized the partially-deuterated analogue, $[Cu_{14}D_{12}(phen)_6(PPh_3)_4][Cl]_2$, which we interrogated using ^{2}H NMR spectroscopy and ESI-MS. We only observed one signal in the ^{2}H NMR spectrum, consistent with the proposed formulation (and the T_d symmetry found in the solid state). In addition, its ESI mass spectrum featured a $[M]^{2+}$ parent ion peak that was shifted by 6 *m/z* versus the signal observed for the protio analogue, as expected for a cluster with only 12 hydride ligands. Finally, we measured the conductivity of Cu_{14}, which was found to be 220.5 $ohm^{-1}\cdot cm^2\cdot mol^{-1}$ in MeCN at room temperature. This value is in excellent agreement

with that expected for a 2:1 electrolyte. With these combined data in hand we were confident that our original formulation, namely, $[Cu_{14}H_{12}(phen)_6(PPh_3)_4][Cl]_2$, was correct.

Overall, this work highlights several themes relevant to the purview of this Account, namely that many complementary techniques must be used to confirm formulation, structure, and analytical purity of APNCs. To our knowledge, this is also first time that conductivity has been applied to nanocluster characterization. Given its ease of implementation and low cost, it could be a valuable and more widely used technique for the characterization of charged nanoclusters. The synthesis of Cu_{14} also illustrates the role that a counterion can play in the determination of reaction outcome. Specifically, Cu_{14} could only be isolated if an appropriate anion (either Cl^- or OTf^-) was present in the reaction mixture. Several other workers have noticed similar effects.[53,61] Perhaps most famously, $[Au_{25}(SCH_2CH_2Ph)_{18}]^-$ could only be formed in the presence of $[N(Oct)_4]^+$, which was added as a phase-transfer reagent.[1] Without addition of $[N(Oct)_4][Br]$, the neutral form of the cluster, $[Au_{25}(SCH_2CH_2Ph)_{18}]$, is isolated instead.[53]

Conclusions and Outlook

Herein, we have described six case studies that highlight several common pitfalls and challenges encountered in APNC synthesis and characterization. Significantly, many of these common pitfalls could have been avoided by adopting a standard characterization protocol, similar to those employed by the organometallic and coordination chemistry communities.[23,24] These pitfalls, and strategies for their mitigation, are summarized in the next two paragraphs.

With respect to synthesis, a majority of the case studies presented here reveal that reducing agents, including the commonly used reagent $NaBH_4$, do not always behave as anticipated. This observation, which has also been noted by others,[62] highlights the need to not only carefully confirm the oxidation state of the final product (with multiple complementary techniques), but to also identify the reaction by-products, as well as the reaction stoichiometry. As part of this process, it is critical to report isolated yields. Too frequently, APNCs are reported in the literature with no yield data. Yields are invaluable for evaluating mass balance, as well as reaction stoichiometry. Indeed, we suggest that editors and reviewers begin to ask for isolated yields as a requirement for publication. It is also apparent that the Brust-Schiffrin protocol is not always beneficial. While Brust-Schiffrin has been a stalwart approach for nanoparticle syntheses for the last 20 years, in two of the nanocluster case studies presented herein the phase-transfer agent apparently played no role in nanocluster formation, and likely just made the isolation of pure material more challenging. It is also clear that many nanocluster syntheses result in the formation of mixtures, as shown in case studies #3 and #5. Because of the challenges inherent in making structure-function relationships of a nanocluster in a mixture, significant effort should be expended to purify APNC samples, and if a mixture cannot be separated, then authors need to acknowledge the presence of impurities in their samples. It is also worth remembering that neither X-ray crystallography nor mass spectrometry can be used to assess bulk purity. In this regard, combustion analysis is underutilized, but potentially powerful, technique for assessing sample purity. Being a bulk characterization technique, it is very sensitive to the presence of impurities (both organic and inorganic) in the sample. HPLC and thin layer chromatography could also be extremely valuable for assessing purity, but are rarely used in APNC analysis. Finally, exposure to oxygen, as seen in case study #4, can also adversely affect APNC reactions. This is expected to be especially true for early and middle 1st row transition metals, such as Fe and Co. As such, the synthesis, work-up, and characterization of these APNCs should be routinely performed under an inert atmosphere.

With respect to characterization, several case studies reveal the peril of over-reliance on a single technique, usually mass spectrometry. Ion silence, ion fragmentation, and reactions with the matrix make the interpretation of mass spectral data more challenging than is often acknowledged. In addition, great care should be taken to faithfully model the isotope patterns and masses of observed mass spectral peaks. We also strongly advise that NMR spectroscopy be routinely employed in nanocluster characterization. The spectral resolution of NMR is unrivalled, and as a result, it can provide information on purity and formulation that are hard to collect with any other technique. Indeed, the use of NMR spectroscopy in case studies #1 and #2 would have quickly identified that the nanocluster syntheses were not proceeding as anticipated. XAS is another powerful method of nanocluster characterization, especially in cases where single crystals for X-ray crystallography are not forthcoming. However, as with any technique, it is important to recognize the limitations of XAS, and to use this technique in tandem with other complementary methods. Indeed, this latter point is probably the most important take-away from this Account, namely, that a wide range of complementary techniques must be employed for nanocluster characterization.

Our goal with the Account is to begin a discussion with respect to the best protocols for nanocluster synthesis and characterization. We believe that adoption of a standard protocol would make APNC synthesis more reliable, thereby accelerating the incorporation of APNCs into a variety of technologies. Ultimately, this latter consequence would benefit us all.

AUTHOR INFORMATION

Corresponding Author

* Email: hayton@chem.ucsb.edu.

Biographical Information

Andrew W. Cook is a doctoral candidate in the Department of Chemistry and Biochemistry at the University of California Santa Barbara. He earned a B.A. in chemistry from Northwestern University in 2014. His research interests include nanocluster synthesis and characterization, along with their catalytic applications.

Trevor W. Hayton is a Professor in the Department of Chemistry and Biochemistry at the University of California Santa Barbara. He received his Ph. D. from the University of British Columbia in 2003. His research interests include organometallics, nanoclusters, and f element coordination chemistry.

Notes

The authors declare no competing financial interest.

ACKNOWLEDGMENT

A. W. C. thanks the Mellichamp Academic Initiative in Sustainability at UCSB for a summer fellowship.

REFERENCES

(1) Jin, R.; Zeng, C.; Zhou, M.; Chen, Y. Atomically Precise Colloidal Metal Nanoclusters and Nanoparticles: Fundamentals and Opportunities. *Chem. Rev.* **2016**, *116*, 10346-10413.
(2) Chakraborty, I.; Pradeep, T. Atomically Precise Clusters of Noble Metals: Emerging Link between Atoms and Nanoparticles. *Chem. Rev.* **2017**, *117*, 8208-8271.
(3) Saillard, J.-Y.; Halet, J.-F. Structure and Bonding Patterns in Large Molecular Ligated Metal Clusters. *Struct. Bond.* **2016**, *169*, 157-179.
(4) Tejada, J.; Chudnovsky, E. M.; del Barco, E.; Hernandez, J. M.; Spiller, T. P. Magnetic qubits as hardware for quantum computers. *Nanotechnology* **2001**, *12*, 181.
(5) Busche, C.; Vilà-Nadal, L.; Yan, J.; Miras, H. N.; Long, D.-L.; Georgiev, V. P.; Asenov, A.; Pedersen, R. H.; Gadegaard, N.; Mirza, M. M.; Paul, D. J.; Poblet, J. M.; Cronin, L. Design and fabrication of memory devices based on nanoscale polyoxometalate clusters. *Nature* **2014**, *515*, 545.
(6) Li, G.; Jin, R. Atomically Precise Gold Nanoclusters as New Model Catalysts. *Acc. Chem. Res.* **2013**, *46*, 1749-1758.
(7) Liu, L.; Corma, A. Metal Catalysts for Heterogeneous Catalysis: From Single Atoms to Nanoclusters and Nanoparticles. *Chem. Rev.* **2018**, *118*, 4981-5079.
(8) Cook, A. W.; Jones, Z. R.; Wu, G.; Scott, S. L.; Hayton, T. W. An Organometallic Cu_{20} Nanocluster: Synthesis, Characterization, Immobilization on Silica, and "Click" Chemistry. *J. Am. Chem. Soc.* **2018**, *140*, 394-400.
(9) Chen, L.-Y.; Wang, C.-W.; Yuan, Z.; Chang, H.-T. Fluorescent Gold Nanoclusters: Recent Advances in Sensing and Imaging. *Anal. Chem.* **2015**, *87*, 216-229.
(10) Colombo, M.; Carregal-Romero, S.; Casula, M. F.; Gutierrez, L.; Morales, M. P.; Bohm, I. B.; Heverhagen, J. T.; Prosperi, D.; Parak, W. J. Biological applications of magnetic nanoparticles. *Chem. Soc. Rev.* **2012**, *41*, 4306-4334.
(11) Higaki, T.; Zhou, M.; Lambright, K. J.; Kirschbaum, K.; Sfeir, M. Y.; Jin, R. Sharp Transition from Nonmetallic Au_{246} to Metallic Au_{279} with Nascent Surface Plasmon Resonance. *J. Am. Chem. Soc.* **2018**, *140*, 5691-5695.
(12) Jin, R. Quantum sized, thiolate-protected gold nanoclusters. *Nanoscale* **2010**, *2*, 343-362.
(13) Beecher, A. N.; Yang, X.; Palmer, J. H.; LaGrassa, A. L.; Juhas, P.; Billinge, S. J. L.; Owen, J. S. Atomic Structures and Gram Scale Synthesis of Three Tetrahedral Quantum Dots. *J. Am. Chem. Soc.* **2014**, *136*, 10645-10653.
(14) Wang, Y.; Zhang, Y.; Wang, F.; Giblin, D. E.; Hoy, J.; Rohrs, H. W.; Loomis, R. A.; Buhro, W. E. The Magic-Size Nanocluster $(CdSe)_{34}$ as a Low-Temperature Nucleant for Cadmium Selenide Nanocrystals; Room-Temperature Growth of Crystalline Quantum Platelets. *Chem. Mater.* **2014**, *26*, 2233-2243.
(15) Gary, D. C.; Flowers, S. E.; Kaminsky, W.; Petrone, A.; Li, X.; Cossairt, B. M. Single-Crystal and Electronic Structure of a 1.3 nm Indium Phosphide Nanocluster. *J. Am. Chem. Soc.* **2016**, *138*, 1510-1513.
(16) Corrigan, J. F.; Fuhr, O.; Fenske, D. Metal Chalcogenide Clusters on the Border between Molecules and Materials. *Adv. Mater.* **2009**, *21*, 1867-1871.
(17) Xie, Y.-P.; Jin, J.-L.; Duan, G.-X.; Lu, X.; Mak, T. C. W. High-nuclearity silver(I) chalcogenide clusters: A novel class of supramolecular assembly. *Coord. Chem. Rev.* **2017**, *331*, 54-72.
(18) Pope, M. T.; Müller, A. *Polyoxometalate Chemistry From Topology via Self-Assembly to Applications*; Springer Netherlands, 2007.
(19) Aiken, J. D.; Finke, R. G. A review of modern transition-metal nanoclusters: their synthesis, characterization, and applications in catalysis. *J. Mol. Catal. A* **1999**, *145*, 1-44.
(20) Zhang, Y.; Hu, Q.; Paau, M. C.; Xie, S.; Gao, P.; Chan, W.; Choi, M. M. F. Probing Histidine-Stabilized Gold Nanoclusters Product by High-Performance Liquid Chromatography and Mass Spectrometry. *J. Phys. Chem. C* **2013**, *117*, 18697-18708.
(21) Xie, S.; Paau, M. C.; Zhang, Y.; Shuang, S.; Chan, W.; Choi, M. M. F. High-performance liquid chromatographic analysis of as-synthesised N,N'-dimethylformamide-stabilised gold nanoclusters product. *Nanoscale* **2012**, *4*, 5325-5332.
(22) Jolly, W. L. *The Synthesis and Characterization of Inorganic Compounds*; Prentice-Hall: Englewood Cliffs, NJ, 1970.
(23) pubs.acs.org/paragonplus/submission/inocaj/inocaj_authguide.pdf (accessed on 08/28/18)
(24) pubs.acs.org/paragonplus/submission/orgnd7/orgnd7_authguide.pdf (accessed on 08/28/18)
(25) Wei, W.; Lu, Y.; Chen, W.; Chen, S. One-Pot Synthesis, Photoluminescence, and Electrocatalytic Properties of Subnanometer-Sized Copper Clusters. *J. Am. Chem. Soc.* **2011**, *133*, 2060-2063.
(26) Nguyen, T. A. D.; Goldsmith, B. R.; Zaman, H. T.; Wu, G.; Peters, B.; Hayton, T. W. Synthesis and Characterization of a Cu_{14} Hydride Cluster Supported by Neutral Donor Ligands. *Chem. Eur. J.* **2015**, *21*, 5341-5344.
(27) Cook, A. W.; Nguyen, T.-A. D.; Buratto, W. R.; Wu, G.; Hayton, T. W. Synthesis, Characterization, and Reactivity of the Group 11 Hydrido Clusters $[Ag_6H_4(dppm)_4(OAc)_2]$ and $[Cu_3H(dppm)_3(OAc)_2]$. *Inorg. Chem.* **2016**, *55*, 12435-12440.
(28) Nguyen, T.-A. D.; Jones, Z. R.; Goldsmith, B. R.; Buratto, W. R.; Wu, G.; Scott, S. L.; Hayton, T. W. A Cu_{25} Nanocluster with Partial Cu(0) Character. *J. Am. Chem. Soc.* **2015**, *137*, 13319-13324.
(29) Nguyen, T.-A. D.; Jones, Z. R.; Leto, D. F.; Wu, G.; Scott, S. L.; Hayton, T. W. Ligand-Exchange-Induced Growth of an Atomically Precise Cu_{29} Nanocluster from a Smaller Cluster. *Chem. Mater.* **2016**, *28*, 8385-8390.
(30) Nguyen, T.-A. D.; Cook, A. W.; Wu, G.; Hayton, T. W. Subnanometer-Sized Copper Clusters: A Critical Re-evaluation of the Synthesis and Characterization of $Cu_8(MPP)_4$ (HMPP = 2-Mercapto-5-n-propylpyrimidine). *Inorg. Chem.* **2017**, *56*, 8390-8396.
(31) *Electrospray Ionization Mass Spectrometry: Fundamentals, Instrumentation, and Applications*; Cole, R. B., Ed.; Wiley: New York, NY, 1997.
(32) Ji, J.; Wang, G.; Wang, T.; You, X.; Xu, X. Thiolate-protected Ni_{39} and Ni_{41} nanoclusters: synthesis, self-assembly and magnetic properties. *Nanoscale* **2014**, *6*, 9185-9191.
(33) Kagalwala, H. N.; Gottlieb, E.; Li, G.; Li, T.; Jin, R.; Bernhard, S. Photocatalytic Hydrogen Generation System Using a Nickel-Thiolate Hexameric Cluster. *Inorg. Chem.* **2013**, *52*, 9094-9101.
(34) Joya, K. S.; Sinatra, L.; AbdulHalim, L. G.; Joshi, C. P.; Hedhili, M. N.; Bakr, O. M.; Hussain, I. Atomically monodisperse nickel nanoclusters as highly active electrocatalysts for water oxidation. *Nanoscale* **2016**, *8*, 9695-9703.
(35) Zhu, M.; Zhou, S.; Yao, C.; Liao, L.; Wu, Z. Reduction-resistant and reduction-catalytic double-crown nickel nanoclusters. *Nanoscale* **2014**, *6*, 14195-14199.
(36) Ivanov, S. A.; Kozee, M. A.; Merrill, W. A.; Agarwal, S.; Dahl, L. F. Cyclo-$[Ni(\mu_2\text{-}SPh)_2]_9$ and cyclo-$[Ni(\mu_2\text{-}SPh)_2]_{11}$: new oligomeric types of toroidal nickel(ii) thiolates containing geometrically unprecedented 9- and 11-membered ring systems. *Dalton Trans.* **2002**, 4105-4115.
(37) Dance, I. G.; Scudder, M. L.; Secomb, R. *c*-$Ni_8(SCH_2COOEt)_{16}$, a receptive octagonal toroid. *Inorg. Chem.* **1985**, *24*, 1201-1208.
(38) Tan, C.; Jin, M.; Zhang, H.; Hu, S.; Sheng, T.; Wu, X. Penta and hexanuclear nickel tiara-like clusters with two different thiolate bridges. *CrystEngComm* **2015**, *17*, 5110-5115.
(39) Daniel, M.-C.; Astruc, D. Gold Nanoparticles: Assembly, Supramolecular Chemistry, Quantum-Size-Related Properties, and Applications toward Biology, Catalysis, and Nanotechnology. *Chem. Rev.* **2004**, *104*, 293-346.
(40) Goulet, P. J. G.; Lennox, R. B. New Insights into Brust−Schiffrin Metal Nanoparticle Synthesis. *J. Am. Chem. Soc.* **2010**, *132*, 9582-9584.
(41) Yang, X.; Shi, M.; Zhou, R.; Chen, X.; Chen, H. Blending of $HAuCl_4$ and histidine in aqueous solution: a simple approach to the Au_{10} cluster. *Nanoscale* **2011**, *3*, 2596-2601.

(42) Paau, M. C.; Hu, Q.; Zhang, Y.; Choi, M. M. F. Role of UHPLC in evaluating as-synthesised ligand-protected gold nanoparticles products. *Anal. Methods* **2015**, *7*, 2452-2457.
(43) Kawasaki, H.; Yamamoto, H.; Fujimori, H.; Arakawa, R.; Iwasaki, Y.; Inada, M. Stability of the DMF-Protected Au Nanoclusters: Photochemical, Dispersion, and Thermal Properties. *Langmuir* **2010**, *26*, 5926-5933.
(44) Ott, L. S.; Finke, R. G. Transition-metal nanocluster stabilization for catalysis: A critical review of ranking methods and putative stabilizers. *Coord. Chem. Rev.* **2007**, *251*, 1075-1100.
(45) Ott, L. S.; Finke, R. G. Nanocluster Formation and Stabilization Fundamental Studies: Investigating "Solvent-Only" Stabilization En Route to Discovering Stabilization by the Traditionally Weakly Coordinating Anion BF_4^- Plus High Dielectric Constant Solvents. *Inorg. Chem.* **2006**, *45*, 8382-8393.
(46) Pollitt, S.; Pittenauer, E.; Rameshan, C.; Schachinger, T.; Safonova, O. V.; Truttmann, V.; Bera, A.; Allmaier, G.; Barrabés, N.; Rupprechter, G. Synthesis and Properties of Monolayer-Protected $Co_x(SC_2H_4Ph)_m$ Nanoclusters. *J. Phys. Chem. C* **2017**, *121*, 10948-10956.
(47) Cook, A. W.; Wu, G.; Hayton, T. W. A Re-examination of the Synthesis of Monolayer-Protected $Co_x(SCH_2CH_2Ph)_m$ Nanoclusters: Unexpected Formation of a Thiolate-Protected Co(II) T3 Supertetrahedron. *Inorg. Chem.* **2018**, *57*, 8189-8194.
(48) Carotenuto, G.; Pasquini, L.; Milella, E.; Pentimalli, M.; Lamanna, R.; Nicolais, L. Preparation and characterization of cobalt-based nanostructured materials. *Eur. Phys. J. B* **2003**, *31*, 545-551.
(49) Kitaev, V. Comment on Effect of Polar Solvents on the Optical Properties of Water-Dispersible Thiol-Capped Cobalt Nanoparticles. *Langmuir* **2008**, *24*, 7623-7624.
(50) Sanghamitra, N. J. M.; Mazumdar, S. Effect of Polar Solvents on the Optical Properties of Water-Dispersible Thiol-Capped Cobalt Nanoparticles. *Langmuir* **2008**, *24*, 3439-3445.
(51) Dreier, T. A.; Ackerson, C. J. Radicals Are Required for Thiol Etching of Gold Particles. *Angew. Chem. Int. Ed.* **2015**, *54*, 9249-9252.
(52) Dreier, T. A.; Compel, W. S.; Wong, O. A.; Ackerson, C. J. Oxygen's Role in Aqueous Gold Cluster Synthesis. *J. Phys. Chem. C* **2016**, *120*, 28288-28294.
(53) Parker, J. F.; Weaver, J. E. F.; McCallum, F.; Fields-Zinna, C. A.; Murray, R. W. Synthesis of Monodisperse $[Oct_4N^+][Au_{25}(SR)_{18}^-]$ Nanoparticles, with Some Mechanistic Observations. *Langmuir* **2010**, *26*, 13650-13654.
(54) Bratsch, S. G. Standard Electrode Potentials and Temperature Coefficients in Water at 298.15 K. *J. Phys. Chem. Ref. Data* **1989**, *18*, 1-21.
(55) Dean, J. A.; Lange, N. A.; Dean, J. A. *Lange's Handbook of Chemistry*; McGraw-Hill, 1992.
(56) Kawasaki, H.; Yamamoto, H.; Fujimori, H.; Arakawa, R.; Inada, M.; Iwasaki, Y. Surfactant-free solution synthesis of fluorescent platinum subnanoclusters. *Chem. Commun.* **2010**, *46*, 3759-3761.
(57) Duchesne, P. N.; Zhang, P. Local structure of fluorescent platinum nanoclusters. *Nanoscale* **2012**, *4*, 4199-4205.
(58) Petty, J. T.; Sergev, O. O.; Ganguly, M.; Rankine, I. J.; Chevrier, D. M.; Zhang, P. A Segregated, Partially Oxidized, and Compact Ag_{10} Cluster within an Encapsulating DNA Host. *J. Am. Chem. Soc.* **2016**, *138*, 3469-3477.
(59) Jordan, A. J.; Lalic, G.; Sadighi, J. P. Coinage Metal Hydrides: Synthesis, Characterization, and Reactivity. *Chem. Rev.* **2016**, *116*, 8318-8372.
(60) Liao, P.-K.; Fang, C.-S.; Edwards, A. J.; Kahlal, S.; Saillard, J.-Y.; Liu, C. W. Hydrido Copper Clusters Supported by Dithiocarbamates: Oxidative Hydride Removal and Neutron Diffraction Analysis of $[Cu_7(H)\{S_2C(aza\text{-}15\text{-}crown\text{-}5)\}_6]$. *Inorg. Chem.* **2012**, *51*, 6577-6591.
(61) Wang, Q.-M.; Lin, Y.-M.; Liu, K.-G. Role of Anions Associated with the Formation and Properties of Silver Clusters. *Acc. Chem. Res.* **2015**, *48*, 1570-1579.
(62) Laxson, W. W.; Özkar, S.; Folkman, S.; Finke, R. G. The story of a mechanism-based solution to an irreproducible synthesis resulting in an unexpected closed-system requirement for the $LiBEt_3H$-based reduction: The case of the novel subnanometer cluster, $[Ir(1,5\text{-}COD)(\mu\text{-}H)]_4$, and the resulting improved, independently repeatable, reliable synthesis. *Inorg. Chim. Acta* **2015**, *432*, 250-257.
.